Oscillation induced worm-like locomotion of carbon nanotubes†

Tung-Wen Cheng,[a] Chieh-Lien Lu,[a] Yao-Chen Lai,[a] Hsin-Fu Kuo,[a] Weileun Fang,[b] Nyan-Hwa Tai[a] and Wen-Kuang Hsu*[a]

Received 1st December 2009, Accepted 12th April 2010
DOI: 10.1039/b925210j

Harmonic oscillation of a doubly clamped single-walled carbon nanotube rope is significantly damped by the resistive force of friction at intertube contacts and the energy transmission rate has been estimated to be lower than that on a metal wire excited at similar frequency and vibrating length by one order of magnitude.

Introduction

The assembly of carbon nanotubes (CNTs) into microscope fibers has drawn much attention in recent years and various fabrication techniques have been developed, including mechanical extrusion, roller spinning and acid assisted injection.[1–3] Compared with individual tubes the tensile strength of CNT fibers is lower by one order of magnitude and the structural weakness has been verified including increased defect density, finite tube length and intertube sliding.[4] CNTs made by catalytic pyrolysis are essentially defective and the tube length mostly distributes at 5–10 μm.[5] Therefore, the CNT fiber strength is mainly controlled by intertube binding, *i.e.* the stronger the intertube strength the greater the effective tensile load transfer to on-tube covalent bonds.[6–8] A recent study has revealed that a CNT suspended between metal islands behaves as an excellent harmonic oscillator and resonance frequency (f_n) can be electrostatically tuned *via* a gate voltage (V_g); the relationship between f_n and V_g being $f_n \propto V_g^2$, $f_n \propto V_g$ and $f_n \propto V_g^{2/3}$ at low, intermediate and high V_g, respectively.[9] So far, little is known about harmonic oscillation of CNT ropes, particularly the bonding character at intertube junctions upon elastic wave propagation remains to be established. In this work, a doubly clamped single-walled CNT (SWCNT) rope is excited at a broad frequency domain and harmonics of resonance frequency are recorded and analyzed according to the classical model. We find that rope oscillation induces a longitudinal stress triggering nanotube migration and elastic wave propagation is therefore dragged by the resistive force of friction at intertube junctions. This outcome explains the observed low energy transmission rate, significant resonance energy (E_{re}) dissipation and high damping factor. Tube movement *via* creeping and buckling mode is also discussed.

[a] *Department of Materials Science and Engineering, National Tsing Hua University, HsinChu 30013, Taiwan. E-mail: wkhsu@mx.nthu.edu.tw; Fax: 886-3-5722366; Tel: 886-3-5715131-35399*
[b] *Department of Power Mechanical Engineering, National Tsing Hua University, No. 101, Section 2, Kuang-Fu Road, Hsinchu 30013, Taiwan. E-mail: fang@pme.nthu.edu.tw; Tel: 886-3-5715731-42923*

† Electronic supplementary information (ESI) available: SWCNT rope with less winding; SEM image of PZT treated rope and oscillation induced structural changes present at the rope surfaces. See DOI: 10.1039/b925210j

Experimental

SWCNTs made by ferrocene pyrolysis are spun into microscope fibers through a spin-nozzle device and three as-made fibers are merged and again twisted into a rope (10 μm in diameter). This yields regular twists along the rope axis and the winding angle revealed by scan electron microscopy (SEM) is *ca.* 60–70°, corresponding to 20–25 turns mm^{-1} (Fig. 1a).[4] Unwinding is prevented by forming networked SWCNTs on the rope surface (Fig. 1a) and fabrication is briefed as follows.

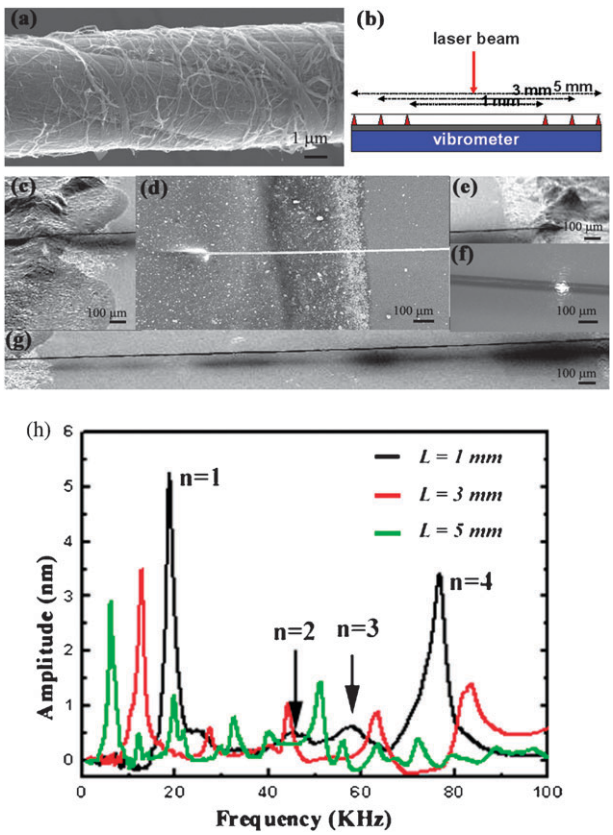

Fig. 1 (a) Twisted SWCNT rope coated networked nanotubes, (b) experimental set up, (c) structure of rope fixed by silver paste (left-end), (d) top view of a fixed-end, (e) structure of SWCNT rope fixed by silver paste (left-end), (f) the laser beam spotted rope, (g) the suspended SWCNT rope. (h) The Φ *vs.* frequency at L = 1 mm (dark), 3 mm (red) and 5 mm (green).

As-made twisted rope is immersed into SWCNTs dispersed in acetone for 5 s and subsequently extracted. This procedure allows transfer of the dispersed SWCNTs onto the rope surfaces and is repeated until the deposited nanotubes are networked. The rope has a linear density (ρ) of 1.76 × 10^{-7} kg m^{-1} and weight ratio between the coating net and the rope is very low (1 × 10^{-4}). The SWCNT rope is stretched and fixed onto a silicon wafer attached to an ultrasonic PZT transducer (Fig. 1b–g) and a low power micro-laser beam (0.1 mW) is employed to measure the rope displacement upon vibration at different string lengths (L = 1, 3 and 5 mm) (Fig. 1f). The stretched rope is excited with a constant power (5 mW) in ambient conditions and the frequency is scanned at 0–100 KHz.

Results and discussion

A doubly clamped string displaces significantly only at resonance frequency and the phenomenon can be well described by the equation below

$$f_n = \frac{n}{2}\sqrt{\frac{T}{\rho L^2}} \qquad (1)$$

where n and T are integer (mode number) and string tension. In the current study, T is produced when a nanotube rope is attached to the substrate and can be determined by inserting the obtained f_n into the equation. Fig. 1h shows vibration amplitudes (Φ) *vs.* frequency at L = 1 mm (dark), 3 mm (red) and 5 mm (green), and the $n \propto L$ is owing to the fact that more resonances are excited when L increases. At L = 1 mm, the fundamental resonance (n = 1) emerges at 20 KHz and other harmonics of resonance frequency (n multiples) are detected at 44 KHz (n = 2), 58 KHz (n = 3) and 78 KHz (n = 4), slightly deviating from the calculated data (*i.e.* 40 KHz, 60 KHz and 80 KHz). The fundamental resonance shifts to a lower frequency domain when L increases and the measurement gives 13 KHz for L = 3 mm and 7 KHz for L = 5 mm, consistent with the prediction by eqn (1). It is noteworthy in the current study that the rope is excited with a constant power so Φ tends to decrease with increasing L and the average is found to be 4 nm at L = 1 mm, 1.5 nm at L = 3 mm and 1 nm at L = 5 mm, accounting for the observed $\Phi \propto L^{-1}$. An insertion of the observed f_n into eqn (1) gives T = 2.5 × 10^{-4}–1 × 10^{-3} N and the wave velocity (ν) appears to be 37.69–75.37 m s^{-1} according to equation $\nu = (T/\rho)^{1/2}$. A previous experiment carried out on a single suspened SWCNT within a vacuum chamber has revealed that the f_n varies with chamber pressure and ν lies on 100–150 m s^{-1}, a value which decreases with air adsorption and is attributable to ρ increase.[9] In our study, the ν reduction by air intercalation between the tubes is unlikely, first, the vibrating main mass comes from the SWCNT rope, and second, the chemisorbed air content is only 0.1 wt%.[10] Accordingly, the lower ν in SWCNT rope relative to the value observed in a single SWCNT possibly arises from large damping and is supported as follows. For SWCNT ropes the structure is held by intertube cohesion and on-tube covalent bonds so f_n detected here is a result of E_{re} transfer between both bonding characters (coupling). Accordingly, the

Table 1 Damping factors for SWCNT rope at various L

ζ_n (×10^{-3})					
1 mm		3 mm		5 mm	
n = 1	n = 2	n = 1	n = 2	n = 1	n = 2
26.1	15.2	30.7	5.4	30	1.8

E_{re} is expected to dissipate at on-tube and intertube oscillators. We have calculated the damping factor (ζ_n) according to the equation $\zeta_n = \Delta f/(2f_n)$ and the bandwidth (Δf) is determined by the half-power points of f_n (Fig. 1h). Table 1 shows ζ at n = 1 and 2, and the average value of various L has been estimated to be 1 × 10^{-2}, greater than the value observed for a single nanotube by one order of magnitude.[11] The question however remains as to what causes a large ζ in the SWCNT rope. For an oscillating SWCNT the elastic wave is primarily transmitted *via* covalent medium and the vibration resonance is controlled by the effective spring constant, *i.e.* $\omega_o = 2\pi f_n = \beta_n^2/2L^2 \cdot [Y(a^2 + b^2)/\rho]^{1/2}$, where a and b are the inner and outer tube diameters, ω_o is the undamped frequency, Y is Young's modulus (100 GPa) and β_n for eigenvalues (1.875).[12] Substitution of the above numbers into the equation yields ω_o = 10^6 Hz, exceeding the current study (0–10^5 Hz) by one order of magnitude. In other words, the on-tube covalent bonds do not damp the rope oscillation below 10^6 Hz and the ν is truly reduced by intertube junctions.

The large ζ found in the SWCNT rope also implies a low energy transmission rate (dK/dt) and equation is expressed as

$$\frac{dK}{dt} = \frac{(\rho\nu\omega^2\Phi^2)\cos^2(kx - wt)}{2} \qquad (2)$$

where $(\rho\nu\omega^2\Phi^2)/2$ is the transmitted energy (E_T), ω is the angular frequency and $k = 2\pi/\lambda$. Table 2 shows dK/dt obtained at n = 1 and 2, and the average E_T is 0.1 mW. For a fixed string the excitation energy (E_{ex}) is the sum of dissipated energy (E_W) and E_T (*i.e.* $E_{ex} = E_T + E_W$), corresponding to the PZT power (5 mW) employed in the current study. Substitution of the obtained E_{ex} and E_T into equation gives E_W = 4.9 mW, indicative of the significant energy dissipation (*i.e.* $E_W \gg E_T$). It is worth mentioning that SWCNT length (L_{tube}) is much shorter than the trench width fabricated in this work so the rope structure is primarily held by intertube binding upon stretching. In this respect, the T obtained here is equivalent to the rope cohesive energy $E_{co} = 0.66[C_o\rho^{-3} + U_o/(8\pi\rho^{2/3})]$, where U_o is the interaction energy per unit length of tube and C_o = 1.02 eV.[4] The equation clearly indicates the ν increase (or ζ decrease) with increasing U_o and tube winding number. We have excited a SWCNT rope with less winding (15 turns mm^{-1}) and the average Δf and ζ are

Table 2 Rate of the energy transmission for the SWCNT rope at various L

dK/dt (×10^{-3})					
L = 1 mm		L = 3 mm		L = 5 mm	
n = 1	n = 2	n = 1	n = 2	n = 1	n = 2
2.62	5.47	1.71	1.54	0.275	0.193

found to be twice those in Fig. 1h (ESI).† This outcome is also consistent with data previously calculated for SWCNT rope strength[4,13], *i.e.* U_o = 0.4 eV for compacted (Fig. 1a) and 0.12 eV for loose ropes (ESI).†

CNTs show the moving activites in an electrostatically charged rope and the tubes only migrate when the bundle exhibits a low packing efficiency within the hexagonal lattice.[14] This is because electron correlation is negligible between the non-aligned tubes, thus lowering E_{co} and the static friction force at intertube contacts. Tube migration is also anticipated in our study, first, SWCNTs are winding and hexagonal packing is therefore unlikely, and second, the E_{re} dissipation *via* resistive intertube friction means an axial stress acting on tubes. So far, tube migration in an oscillating rope has not been reported and the observations above seem to suggest that the tube moves as a result of oscillation induced stress formation. For an oscillating system the return of displaced string to equilibrium relies on the structural elasticity and our simulation carried out at $\Phi \neq 0$ shows a distinguishable C–C bond extension along the *a*-axis. Simulation is carried out as follows, first, a SWCNT bundle (51.12 Å in length, atomic number = 240) is built within a 5 × 5 nm window and the central and surrounding spiral tubes (5,0) are spaced by 3.115 Å (top, Fig. 2a), second, the density functional theory is treated with exchange–correlation and Perdew-Ultrasoft pseudo-potentials, and the SCF tolerance threshold is set at 10^{-6} eV/atom for structural convergence and 0.04 $Å^{-1}$ for the Monkhorst–Pack *k*-point grid separation, third, the potential energy of each atom is derived from the COMPASS force field and the cut-off distance between non-bonded atoms is set at 15.50 Å, fourth, the tube is stretched (σ = 10 GPa) simultaneously along [100] and [$\bar{1}$00] directions so the structure remains unchanged at the center of mass [000]; and fifth, the time-frame for stress relaxation is set at 36 fs. We find that

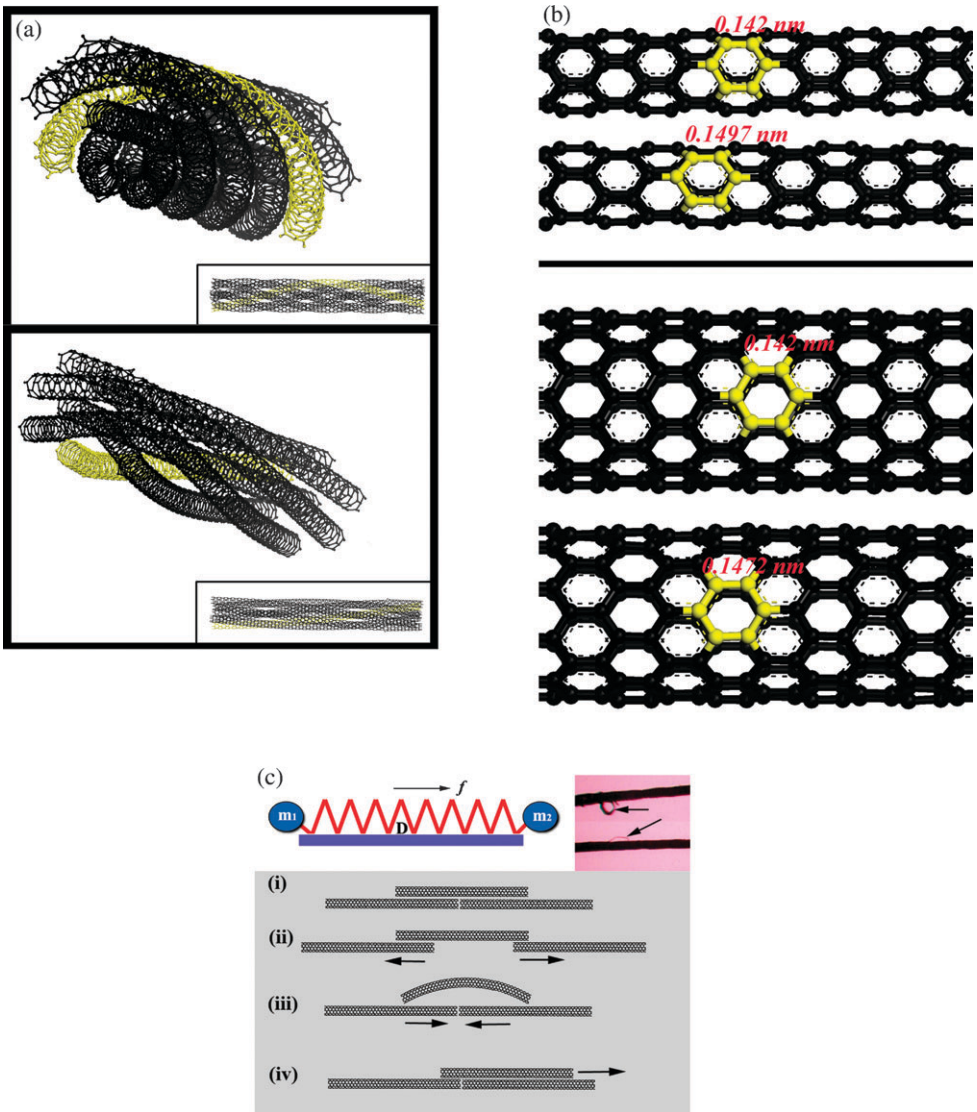

Fig. 2 (a) (top) Simulated packed SWCNTs before structural optimization (yellow highlights spiral tube). (lower) Simulated packed SWCNTs after structural optimization. (b) Tube axial extension upon stress application for (5,0) (top) and (10,0) tubes (lower). The yellow highlights the relative movement of hexagonal ring at relaxed (top panel) and stressed states (lower panel). (c) A worm-like locomotion mechanism for tube migration (i-iv). Insert: a damped spring model linked with two masses (top left) and optical images of closed loops at rope surface (top right).

packed SWCNTs become loose after structural optimization and the pitch decreases from 0.0125 to 0.009 turns per nm, attributable to tube flexibility (lower, Fig. 2a). The loose bundle structure however facilitates tube sliding within the rope and will be discussed in the text. At a stressed state the C–C bond is lengthened by 5.38% and retracts to 1.42 Å upon stress release (*i.e.* $\Phi = 0$) (top, Fig. 2b). For a larger tube (10,0) the C–C bond extension decreases to 3.64% and the underlying mechanism is due to the fact that increasing sp^2 characters along the tube circumference enhances the resisting force to tensile stress (lower, Fig. 2b). The differentiated elongation (α) becomes significant when L_{tube} increases and we find $\alpha = 17.4$ nm at $L_{tube} = 1$ μm and $\alpha = 34.8$ nm at 3 μm, exceeding the threshold value for the tube bending (8–12 nm).[15] In practice, the rope consists of finite SWCNTs packed closely so the tubes are expected to elongate and contract in the presence of mechanical interlocking. In this respect, the tubes possibly remain stretched at $\Phi = 0$ and relaxation may proceed through elastic creeping within the intertube voids. The phenomenon can be modelled as a damped spring linked with two masses and the equation is expressed as $\boldsymbol{f} = k(x' - x'') - D\mathrm{d}x/\mathrm{d}t$, where $\boldsymbol{f}$ is force along spring direction, D is damping (or interlocking force in this study), k is spring force constant ($\sim 10^5$ dynes cm^{-1} for C=C bond), and x' and x'' are the spring length at relaxed and stressed states, corresponding to α (top left, Fig. 2c). The equation has been used to describe the motion dynamics of snakes and worms, and the muscle contraction and anisotropic friction were realized as primary motive forces upon forward sliding.[16] In our study, the force acting on tubes comes mainly from T and the rope remains unfractured upon oscillation, indicative of $T\cos\theta \approx \boldsymbol{f} < D$ where θ is the tube winding angle in the rope. Based on experimental data the average θ is set as 25° and $\alpha = 17 \sim 34$ nm so the tube mobility ($\mathrm{d}x/\mathrm{d}t$) can be evaluated through the friction energy equation $E_W = [\mu_k \int F(x)\mathrm{d}x]/t$ where F and μ_k are the maximum static friction force at the tube–tube contact ($= 1.4 \times 10^{-4}$ N) and the coefficient of kinetic friction ($= 0.1$).[4,13] We find $x/t = 12.25$ nm s^{-1}, lower than the intershell motion by 12 orders of magnitude.[17] Calculation then gives $D = 0.013$–0.027 N, exceeding F by two orders of magnitude. In other words, $\alpha \neq 0$ truly occurs at $\Phi = 0$ by winding induced interlocking and $\alpha > 0$ and $\alpha > 0$ represent the tube in stretched and compressed states respectively. Based on the analyses above we believe that the tubes migrate *via* a buckling mode and that is supported by closed loop formation at the rope surface (top right, Fig. 2c) and topograpical variation at the rope surfaces (ESI).† Fig. 2c shows a bundle consisting of three SWCNTs and similar aggregation is often detected in the rope sample. Upon rope stretching the inter-gap along the bundle axis increases whereas the upper tube remains as linkage over the strained tubes (i–ii). When the rope displaces to equilibrium the linkage is compressed and tends to buckle (ii–iii). According to Euler's law the force ($\boldsymbol{f_B}$) applied at the tube where bending occurs is given by $\boldsymbol{f_B} = \pi^2 YI/L_{tube}$, where I is the inertia moment of the tube cross section, corresponding to $\pi r^3 t$. For SWCNTs the tube wall thickness (t) is constant and the factor that controls tube bending is therefore determined by L_{tube} and the tube radius (r). A similar deformation has previously been detected in CNT-polymer composites and the critical L_{tube}/r ratio for tube bending upon compression by the surrounding matrix was found to be 10.5.[18] In the current study, r lies on $0.6 \sim 0.8$ nm and α available for bending is 25 nm, thus giving $L_{tube}/r = 31 \sim 40$ in the current study. The buckled tube is straightened when the rope again displaces and slides to $\alpha = 0$ (iii–iv). If tube buckling however exceeds the critical angle (50–60°) the kinking mode emerges and straightening *via* elastic creeping would be unlikely.[15] This develops a closed loop upon rope oscillation, consistent with Fig. 2c (top right).

Experiments were also carried out on a PAN-based carbon fiber (CF) with a similar diameter (insert, Fig. 3a), and the average ζ is found to be much lower compared with the SWCNT rope, *i.e.* $\zeta_n = 4.6$ ($n = 1$) and 3.6 ($n = 2$) at $L = 1$ mm, 4.4 ($n = 1$) and 3.4 ($n = 2$) at $L = 3$ mm, and 8.7 ($n = 1$) and 3.1 ($n = 2$) at $L = 5$ mm. Note that CF has a comparable ρ and T ($\sim 3 \times 10^{-3}$ N) with SWCNTs so small ζ is attributable to low E_{re} dissipation. Fig. 3b plots E_{re} at $L = 1$ mm based on equation $E_{re} = k\Phi^2 m/2 \cdot (e^{-\zeta/m})$ where m is the string mass and ζ is obtained from Table 1. At $n = 1$, the E_{re} storage in oscillating CF is greater by fivefold relative to the SWCNT rope, supporting a low dissipation process. When the mode number increases E_{re} is carried by a multi-oscillator, thus reducing the E_{re} magnitude. For the SWCNT rope, the E_{re} is very small and remains below 20 pJ throughout, again verifying a significant dissipation. Additional evidence in support of low E_{re} dissipation in CF comes from the fact that the material mainly consists of continuous graphene sheets

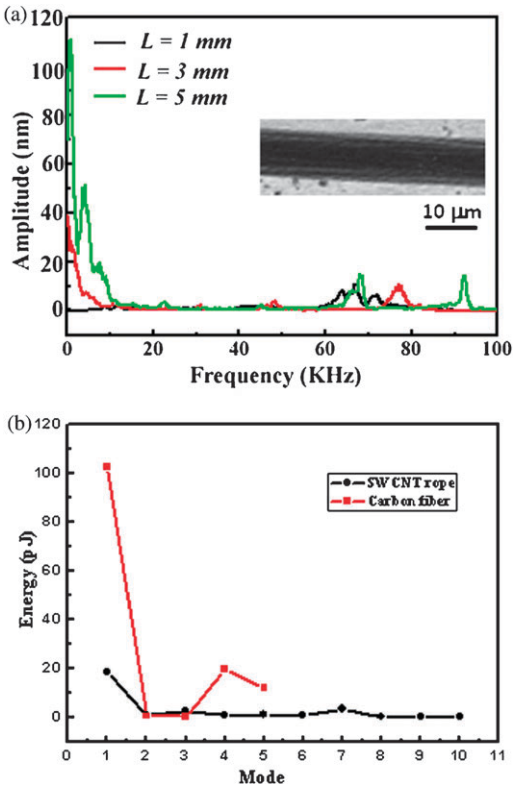

Fig. 3 (a) Φ *vs.* frequency at $L = 1$ mm (dark), 3 mm (red) and 5 mm (green) for CF: insert shows SEM image of CF. (b) E_{re} storage in the oscillating SWCNT rope (dark) and CF (red).

oriented along the fiber axis so damping *via* the interlayer sliding known to occur only at high temperature is relatively difficult compared with intertube motion.[19]

We thank the National Science Council of Taiwan for financial support (NSC-97-2112-M-007-014-MY2).

References

1 B. Vigolo, A. Pénicaud, C. Coulon, C. Sauder, R. Pailler, C. Journet and P. Bernier P. Poulin, *Science*, 2000, **290**, 1331.
2 Y. L. Li, I. A. Kinloch and A. H. Windle, *Science*, 2004, **304**, 276.
3 L. M. Ericson, H. Fan, H. Peng, V. A. Davis, W. Zhou, J. Sulpizio, Y. Wang, R. Booker, J. Vavro, C. Guthy, A. N. G. Parra-Vasquez, M. J. Kim, S. Ramesh, R. K. Saini, C. Kittrell, G. Lavin, H. Schmidt, W. W. Adams, W. E. Billups, M. Pasquali, W. -F. Hwang, R. H. Hauge, J. E. Fischer and R. E. Smalley, *Science*, 2004, **305**, 1447.
4 T. W. Cheng and W. K. Hsu, *Appl. Phys. Lett*., 2007, **90**, 123102.
5 P. C. P. Watts, W. K. Hsu, H. W. Kroto and D. R. M. Walton, *Nanoletters*, 2003, **3**, 549.
6 M. Zhang, K. R. Atkinson and R. H. Baughman, *Science*, 2004, **306**, 1358.
7 B. I. Yakobson, *Appl. Phys. Lett*., 1998, **72**, 918.
8 C. Jourrnet, W. K. Maser, P. Bernier, A. Loiseau, M. Lamy, M. L. de la Chapelle, S. Lefrant, P. Deniard, R. Lee and J. E. Fischer, *Nature*, 1997, **388**, 756.
9 V. Sazonova, Y. Yaish, H. ŰSTűNEL, D. Roundy, T. A. Arias and P. McEuen, *Nature*, 2004, **431**, 284.
10 K. Atkinson, S. Roth, M. Hirscher and W. Grünwald, *Fuel Cells Bull*., 2001, **4**, 9.
11 S. J. Papadakis, A. R. Hall, P. A. Williams, L. Vicci, M. R. Falvo, R. Superfine and S. Washburn, *Phys. Rev. Lett*., 2004, **93**, 146101.
12 M. M. Treacy, T. W. Ebbesen and J. M. Gibson, *Nature*, 1996, **381**, 678.
13 S. H. Syue, S. Y. Lu, W. K. Hsu and H. C. Shih, *Appl. Phys. Lett*., 2006, **89**, 163115.
14 S.-H. Syue, C.-T. Hsu, U.-S. Chen, H.-J. Chen, W.-K. Hsu and H.-C. Shih, *Carbon*, 2009, **47**, 1239.
15 S.-Y. Lu and W.-K. Hsu, *ChemPhysChem*, 2005, **6**, 1040.
16 Gavin S. P. Miller, *ACM SIGGRAPH Comput. Graphics*, 1988, **22**(4), 169.
17 Y. Zhao, C.-C. Ma, G.-H. Chen and Q. Jing, *Phys. Rev. Lett*., 2003, **91**, 175504.
18 O. Lourie, D. M. Cox and H. D. Wagner, *Phys. Rev. Lett*., 1998, **81**, 1638.
19 L. A. Girifalco, M. Hodak and R. S. Lee, *Phys. Rev. B: Condens. Matter Mater. Phys*., 2000, **62**, 13104.

